# Optimal control of the electric susceptibility of a molecular gas by designed nonresonant laser pulses of limited amplitude

Liyang Shen, S. Shi,[a] and H. Rabitz
*Department of Chemistry, Princeton University, Princeton, New Jersey 08544*

C. Lin and M. Littman
*Department of Mechanical and Aerospace Engineering, Princeton University, Princeton, New Jersey 08544*

J. P. Heritage
*Department of Electrical Engineering, University of California at Davis, Davis, California 95616*

A. M. Weiner[b]
*Bellcore, 331 Newman Springs Road, Red Bank, New Jersey 07701*

(Received 17 August 1992; accepted 4 February 1993)

We present a theoretical study on optimal control of the electric susceptibility change of a homogeneous molecular gas resulting from orientational anisotropy induced by nonresonant lasers with limited intensity. It is assumed that the molecular gas is initially in thermal equilibrium. Two types of optimal control objectives have been considered: terminal control and temporal profile control (i.e., trajectory control). A step function is introduced into the cost functionals which successfully helps to realize the restriction on the magnitude of the field amplitude in numerical optimization, as demonstrated by the examples. Calculations are carried out for $CS_2$ which has a small rotational constant ($B = 0.1091\ cm^{-1}$) and a quite large polarizability anisotropy ($\Delta\alpha = 9.6\ Å^3$). For terminal control of a maximal susceptibility change at a target time $T$, it is found that the optimal control field is composed of a series of rectangular pulses with identical amplitudes equal to a preassigned bound value. All of the optimal fields for terminal control are functions of $(T-t)$ over the time interval $[0,T]$ with characteristic time $1/8B$ and period $1/2B$. For temporal profile control, the degree of control is strongly dependent on the length of time interval over which a target profile is defined. Usually, if a time interval is shorter than $1/8B$ and a target profile is a smooth and non-negative function with a reasonable maximal value, the control can be achieved perfectly. In other cases the detailed assignment of the weight function in the cost functional plays an important role in determining how to make an optimally controlled susceptibility change profile approach the target profile. Furthermore, we have also examined the temperature effects on optimal control in this paper. It can be shown that the general optimal control properties observed by $CS_2$ will also be valid for other linear molecular gases with small rotational constants.

## I. INTRODUCTION

Recently, there has been increasing interest in the control of molecular dynamics by appropriately designed electromagnetic pulses. A wide variety of physical objectives are currently under extensive study including magnetic resonance selective excitations,[1,2] crystal lattice vibrations,[3] population inversion[4] and population transfer,[5] molecular rotational,[6] vibrational,[7–12] and selective chemical reactions.[13–17] Much useful information about controlled dynamics has been provided, and the work also has indicated why previous attempts, with only monochromatic or simple laser fields, did not give very encouraging results. A basic conclusion is the necessity to *design* optimal fields to achieve efficient control.

A number of theoretical treatments have suggested intelligently designing laser fields to enhance control efficiency. For example, for selective dissociation of a molecule, Rice and Tannor[14] proposed a simple pump-and-dump scheme with two ultrashort laser pulses. The numerical results show that the selectivity of product formation can be enhanced by carefully selecting the time delay between the pump and dump pulses. On the other hand, Shapiro and Brumer[18] suggested a two coherent path scheme to control the relative product yield by adjusting the relative phase of two coherent excitation laser pulses. Recently, Gordon's experiment for HCl multiphoton ionization indicated that this scheme may work for some favorable systems.[18]

A more systematic method within the framework of optimal control theory has been successfully applied in various theoretical control studies of quantum dynamical systems.[6,7,13,15] For the given physical objectives and penalties,

[a]Present address: Biosym Technologies, Inc., San Diego, California 92121.

[b]Present address: School of Electrical Engineering, Purdue University, West Lafayette, Indiana 47907.

 0021-9606/93/107792-12$06.00 

such as energy fluence, an appropriate cost functional is formulated. The optimal field is designed to minimize this functional. The optimal control studies so far have focused on terminal control, i.e., achievement of a physical observable at a target time $T$. The controlled evolution profile of a physical observable (i.e., trajectory control) has not yet been explored. From a control point of view, control of the observable along a trajectory is more difficult since it requires the observable to track a given function of time. Physically, it is important to study this type of control because of its potential applications to a wide range of physical systems, e.g., controlling molecular orientation for collision dynamics[19] as well as for optical gate studies,[20] etc. Furthermore, control of this type should lead to a better understanding of the dynamical capabilities of a molecule. Therefore, there is strong motivation to explore microsystem optimal control of a physical observable tracking a temporal functional form.

In this paper, we present theoretical studies on the optimal control of the electric susceptibility change of a molecular gas resulting from orientational anisotropy induced by nonresonant laser pulses with limited amplitude. The main purpose is to seek for the possibility of molecular control using existing laser and pulse shaping technology. The optimal control of the electric susceptibility change of a molecular gas is potentially demonstrable in the laboratory with currently available experimental techniques. First, a nonresonant laser can induce a rotational anisotropy through interaction with the induced molecular dipole moments. The advantage of using a laser, instead of a microwave source, to control molecular rotations is that laser fields can possess higher intensity and can be precisely shaped and of ultrashort duration.[21,22] The typical frequency band width required for most molecular rotational transitions at room temperature, such as for $CS_2$, is less than a few hundred wave numbers. Laser pulses with durations in the range of 30–100 fs, with frequency bandwidths from $\sim$100–350 $cm^{-1}$, are available from various laser systems.[23] Using special nonlinear pulse compression techniques, optical pulses as short as 6 fs, with bandwidths approaching 2000 $cm^{-1}$, have also been generated.[24] Thus laser pulses can provide sufficient bandwidths to drive molecular rotations and ultimately vibrations. Second, precise techniques for femtosecond pulse shaping and wave form synthesis, which could be used to create the actual laser wave forms required for optimal control experiments, have been demonstrated.[21,22] Typically pulse shaping experiments have been performed with pulses 75–100 fs in duration or longer, but recently shaping of laser pulses as short as 20 fs has also been achieved.[25] Thirdly, high quality Hamiltonians for molecular rotation and radiative interaction coefficients are available, since rotational constants and molecular polarizabilities in the ground electronic and vibrational states are accurately known for many molecules. Finally, for a linear or symmetric-top molecular gas, the electric susceptibility change can be probed by birefringence measurements. The temporal birefringence change of $CS_2$ gas was observed by Heritage and co-workers.[26] In their experiment, a single ultrashort ($\sim$0.8 ps) nonresonant laser pulse with wavelength 1.06 $\mu$m was used to pump $CS_2$ to create a coherent superposition of rotational states, and another weak pulse with wavelength 0.53 $\mu$m was employed as the probe field. The temporal birefringence is determined by measuring the energy of the probe laser transmitted through the analyzing polarizer as a function of the probe–pulse delay. They also showed computationally that the response of the susceptibility change of $CS_2$ gas to various sinusoidal or Gaussian shaped pump pulses is different.[27]

In this paper, we focus on both terminal and temporal profile control of the electric susceptibility. Additional cost penalties are included on the laser energy fluence and field amplitude. The molecular gas is assumed to be initially in thermal equilibrium. The control takes place in the picosecond range, which is much shorter than gas collision times at STP. Accordingly, the collisionless Schrödinger equation can be utilized to describe the evolution of gas molecules.

The present paper is organized as follows. In Sec. II, we describe the physical system and the electric susceptibility. The cost functionals are formulated, and the working formulas are then derived for numerical calculation. In Sec. III, as an illustrative example, $CS_2$ gas is studied and the optimal susceptibility changes and the optimal control fields are presented. Finally, some concluding remarks are given in Sec. IV. Atomic units are used throughout paper, unless stated otherwise.

## II. FORMALISM

### A. The system and electric susceptibility

The system considered is a homogeneous molecular gas characterized as initially being in a Boltzmann distribution. The molecules, treated as rigid rotors, can be linear, symmetric-tops, or asymmetric-tops. The driving laser field is $Z$ polarized with the form

$$\epsilon(t)=A(t)\cos[\omega_0 t+\vartheta(t)], \tag{2.1}$$

where $\omega_0$ is the nonresonant carrier frequency, which is larger than the molecular vibrational frequencies and smaller than any accessible electronic transition frequencies. $\vartheta(t)$ is the phase of the field and $A(t)$ is the amplitude which is a real function. The physical observable to be controlled is the electric susceptibility along the field direction, $\kappa(t)$, which is defined as the mean value of the molecular polarizability, $\alpha_z$, along the field direction

$$\begin{aligned}\kappa(t)&=N_d\,\mathrm{Tr}[\alpha_z\ \rho(t)]\\&=N_d\,\mathrm{Tr}[(\Delta\alpha\cos^2\theta+\alpha_\perp)\rho(t)],\end{aligned} \tag{2.2}$$

with

$$\alpha_\perp=\alpha_a+(\alpha_b-\alpha_a)\cos^2\chi, \tag{2.3}$$

and

$$\Delta\alpha=\alpha_c-\alpha_\perp\ . \tag{2.4}$$

Here $\rho(t)$ is the density operator of the gas, $N_d$ is the number density of the molecular gas, $\alpha_a$, $\alpha_b$, and $\alpha_c$ are the

molecular polarizabilities along three principle axes *a*, *b*, and *c*, respectively, and $\theta$, $\phi$, and $\chi$ are the molecular Euler angles.[28]

The interaction Hamiltonian operator for the system is

$$H_i(t) = -\tfrac{1}{2}\alpha_z A^2(t)\cos^2[\omega_0 t + \vartheta(t)]. \tag{2.5}$$

Because of rapid oscillation of $\cos[\omega_0 t+\vartheta(t)]$, one can average $H_i(t)$ over a few optical cycles to obtain the effective interaction Hamiltonian

$$H_I(t) = -\tfrac{1}{4}\alpha_z A^2(t). \tag{2.6}$$

The dynamical equation for the density operator, $\rho_I(t)$, in the interaction representation is

$$i\frac{\partial \rho_I(t)}{\partial t} = [H_{\rm int}(t), \rho_I(t)] \tag{2.7}$$

with

$$\rho_I(t) = \exp(iH_0 t)\rho(t)\exp(-iH_0 t) \tag{2.8}$$

and

$$H_{\rm int}(t) = \exp(iH_0 t)H_I(t)\exp(-iH_0 t), \tag{2.9}$$

where $H_0$ is the field-free rotational Hamiltonian. It is assumed that initially the gas is in thermal equilibrium at temperature $T_m$. Therefore, the density operator at $t=0$ has the form

$$\rho(0) = \exp(-H_0/kT_m). \tag{2.10}$$

Let the density operator, $\rho_I(t)$, at time $t$ be written as

$$\rho_I(t) = \rho_I^{(0)}(t) + \rho_I^{(1)}(t) + \cdots, \tag{2.11}$$

where $\rho_I^{(k)}(t)$, $(k=0,1,\ldots)$, are defined as the $k$th-order perturbation solutions in terms of the field strength. Substituting this equation into Eq. (2.7), we can obtain a set of equivalent dynamical equations

$$i\frac{\partial \rho_I^{(0)}(t)}{\partial t} = 0, \tag{2.12}$$

and

$$i\frac{\partial \rho_I^{(k)}(t)}{\partial t} = [H_{\rm int}(t), \rho_I^{(k-1)}(t)] \quad \text{for} \quad k \geqslant 1. \tag{2.13}$$

The zero-order solution is

$$\rho_I^{(0)}(t) = \rho(0), \tag{2.14}$$

and the first-order solution is

$$\begin{aligned}\rho_I^{(1)}(t) &= -i\int_0^t [H_{\rm int}(t'), \rho(0)]\,dt' \\ &= \frac{i}{4}\int_0^t A^2(t') e^{iH_0 t'}[\alpha_z, \rho(0)]e^{-iH_0 t'}\,dt'.\end{aligned} \tag{2.15}$$

When the interaction energy is small and the controlling time, $T$, is short, such that $|H_{\rm int}|T \ll 1$, we may ignore the higher order perturbation solutions

$$\rho_I(t) \simeq \rho_I(0) + \rho_I^{(1)}(t). \tag{2.16}$$

Then, the susceptibility in Eq. (2.2) becomes

$$\kappa(t) = N_d \,\mathrm{Tr}[\alpha_z e^{-iH_0 t}\rho_I(t)e^{iH_0 t}]. \tag{2.17}$$

The first term of $\rho_I(t)$ in Eq. (2.16), $\rho_I(0)$, gives rise to the initial susceptibility, $\kappa(0)$, and thus the susceptibility change reads

$$\Delta\kappa(t) = N_d \,\mathrm{Tr}[\alpha_z e^{-iH_0 t}\rho_I^{(1)}(t)e^{iH_0 t}]. \tag{2.18}$$

To calculate the trace, one may choose the eigenfunctions of $H_0$ as a basis set, in which both $H_0$ and $\rho(0)$ are diagonal. The eigenfunctions of $H_0$ can be denoted by $|lnm\rangle$,

$$H_0|lnm\rangle = E_{ln}|lnm\rangle \tag{2.19a}$$

with

$$|lnm\rangle = \sum_{k=-l}^{l} \beta_{nk}|lkm\rangle. \tag{2.19b}$$

Here $l$ is the quantum number of total angular momentum, $m$ and $k$ are the components of $l$ along the $Z$ axis and $c$ axis, and $n$ is just a label. For a symmetric-top molecule, $n$ is equal to $k$, and $\beta_{nk}$ are delta functions, $\beta_{nk}=\delta_{nk}$. For a linear molecule the summation disappears and one has $n=k\equiv 0$. It can be shown that the diagonal elements of the first-order density matrix $\rho_I^{(1)}(t)$ are zero. This implies that the population distribution is not changed to first order. After some algebra, Eq. (2.18) becomes

$$\Delta\kappa(t) = \int_0^t A^2(t-s)\tilde{T}(s)\,ds, \tag{2.20a}$$

where

$$\begin{aligned}\tilde{T}(s) = \frac{iN_d}{4}\sum_{lnml'n'} |(\alpha_z)^{ln}_{l'n'}(m)|^2[\rho_{ln}(0) \\ - \rho_{l'n'}(0)]\exp(i\omega_{lnl'n'}s).\end{aligned} \tag{2.20b}$$

with

$$(\alpha_z)^{ln}_{l'n'}(m) = \langle lnm|\alpha_z|l'n'm\rangle \tag{2.20c}$$

and

$$\omega_{lnl'n'} = E_{ln} - E_{l'n'}. \tag{2.20d}$$

Here $\rho_{ln}(0)$ is the initial probability in state $|lnm\rangle$. Equation (2.20a) shows that for a nonresonant laser field of normal intensity, the susceptibility change of a molecular gas only depends on the square of the amplitude, $A^2(t)$.

For a gas of linear molecules, one has

$$\Delta\kappa(t) = N_d\Delta\alpha \,\mathrm{Tr}[\cos^2(\theta)e^{-iH_0 t}\rho_I^{(1)}(t)e^{iH_0 t}] \tag{2.21a}$$

and

$$\begin{aligned}\tilde{T}(s) = N_d\Delta\alpha \,\mathrm{Im}\Big[&\exp(-i2\pi 10Bs) \\ &\times \sum_{j=0}^{\infty} G_{2j+1}\exp(-i2\pi 8Bjs) + \exp(-i2\pi 6Bs) \\ &\times \sum_{j=0}^{\infty} G_{2j+2}\exp(-i2\pi 8Bjs)\Big]\end{aligned} \tag{2.21b}$$

with

$$G_l=\Delta\alpha\frac{W_s(l)}{15Z_p}\frac{l(l-1)}{(2l-1)}\{\exp[-l(l-1)/a]-\exp[-(l-2)(l-1)/a]\},\tag{2.21c}$$

where $a=kT_m/B$, $Z_p$ is rotational partition function and Im denotes taking the imaginary part. $W_s(l)$ is equal to the number of nuclear spin functions that couple with $l$. For example, suppose the molecules are homonuclear diatomic. Then for integral spin $I$,

$$W_s(l)=\begin{cases}I(2I+1) & \text{for odd } l,\\ (I+1)(2I+1) & \text{for even } l,\end{cases}$$

while for half-integral spin $I$,

$$W_s(l)=\begin{cases}(I+1)(2I+1) & \text{for odd } l,\\ I(2I+1) & \text{for even } l.\end{cases}$$

Since the frequency difference of successive transitions for both even $l$ states and odd $l$ states is a constant $8B$, the two summations in Eq. (2.21b) can be conveniently performed by using the fast Fourier transform (FFT) algorithm. From Eq. (2.21b) it is seen that $\tilde{T}(s)$ is a periodic function of $s$ with a period $1/2B$.

### B. Optimal control formulas

Following the prescription of optimal control theory,[29] one starts an optimal control calculation by setting up a cost functional in accordance with the physical objectives. As mentioned in Sec. I, there are two types of control objectives: (1) terminal susceptibility control where a specified value of the susceptibility change is to be reached at a target time $T$; (2) susceptibility functional form control where a specified functional form for the susceptibility change is desired as a function of time. Two physical restrictions on the pump laser field are taken into account: the total energy fluence and peak intensities [or the norm of the amplitude, $|A(t)|$]. Experimentally, the fluence is limited by the femtosecond laser/amplitude system. After pulse shaping, the fluence is at most equal to the fluence supplied by the laser. For a given fluence, the peak intensity can vary substantially depending on the duration and the structure of the shaped laser wave form. In some experiments it is desirable to limit the peak intensity in order to avoid unwanted, parasitic nonlinear effects or sample damage. Accordingly, two cost functionals and optimization formulae will be given in the following two subsections.

#### 1. Terminal susceptibility control

There are a number of different ways to account for the restriction on the amplitude of the fields for numerical optimization. Here let $A_0$ be a given upper bound value for $|A(t)|$. We introduce a restraint functional

$$L_p=\beta_1\int_0^T[A(t)-A_0]^2\,h[A(t)-A_0]dt+\beta_2\int_0^T[-A(t)-A_0]^2\,h[-A(t)-A_0]dt,\tag{2.22a}$$

where the amplitude $A(t)$ is to be optimized. Instead of $A(t)$, we can directly optimize $A^2(t)$. In this case, the restraint functional can be expressed as

$$L_p=\beta_1\int_0^T[A^2(t)-A_0^2]^2\,h[A^2(t)-A_0^2]dt+\beta_2\int_0^T[-A^2(t)]^2\,h[-A^2(t)]dt.\tag{2.22b}$$

Here $\beta_1$ and $\beta_2$ in Eqs. (2.22a) and (2.22b) are weight factors and $h(x)$ is a Heaviside function defined by

$$h[x]=\begin{cases}1 & \text{for } x\geqslant 0,\\ 0 & \text{for } x<0,\end{cases}\tag{2.22c}$$

and thus Eq. (2.22a) and Eq. (2.22b) weight against $|A(t)|>A_0$. Note that strictly speaking, the last term in Eq. (2.22b) is zero, but when using $B(t)=A^2(t)$ as the actual control variable, there is no assurance that the algorithm will pick $B(t)>0$. Thus, the last term is included so that solutions with $B(t)>0$ are obtained. The cost functional $Q$ reads

$$Q=\beta_0[\Delta\kappa(T)-f_0]^2+\beta_f L_f+L_p\tag{2.23}$$

with the energy fluence penalty term

$$L_f=\int_0^T A^2(t)dt,\tag{2.24}$$

where $f_0$ is a target value of the susceptibility change at $T$. The weight factors $\beta_0$, $\beta_f$, $\beta_1$, and $\beta_2$ are used for balancing the relative importance of each term. Including the term, $L_f$, in the cost functional expresses the desire to minimize the energy fluence of the field. The functional derivative of $Q$ with respect to $A(t')$ using Eq. (2.22a) has the form

$$\frac{\delta Q}{\delta A(t')}=\begin{cases}4\beta_0[\Delta\kappa(T)-f_0]\tilde{T}(T-t')A(t')+\dfrac{\delta(\beta_f L_f+L_p)}{\delta A(t')} & \text{for } 0<t'<T,\\ 0 \quad \text{otherwise,}\end{cases}\tag{2.25a}$$

with

$$\frac{\delta(\beta_f L_f+L_p)}{\delta A(t')}=2\beta_1[A(t')-A_0]h[A(t')-A_0]+2\beta_2[A(t')+A_0]h[-A(t')-A_0]+2\beta_f A(t').\tag{2.25b}$$

Similarly using Eq. (2.22b) the functional derivative with respect to $A^2(t)$ is

$$\frac{\delta Q}{\delta A^2(t')}=\begin{cases}2\beta_0[\Delta\kappa(T)-f_0]\tilde{T}(T-t')+\dfrac{\delta(\beta_f L_f+L_p)}{\delta A^2(t')} & \text{for } 0<t'<T,\\ 0 \quad \text{otherwise,}\end{cases} \tag{2.26a}$$

with

$$\frac{\delta(\beta_f L_f+L_p)}{\delta A^2(t')}=2\{\beta_1[A^2(t')-A_0^2]h[A^2(t')-A_0^2]+\beta_2 A^2(t')h[-A^2(t')]\}+\beta_f. \tag{2.26b}$$

Equations (2.26) and (2.25) are the working formulas to search for the optimal field $A^2_{\rm op}(t')$ and $A_{\rm op}(t')$, respectively. The optimal field, $A^2_{\rm op}(t)$ [or $A_{\rm op}(t)$], can be obtained by solving the equation, $\delta Q/\delta A^2(t')=0$ [or $\delta Q/\delta A(t')=0$], iteratively. It should be noted that the optimal solution may not be unique (i.e., $Q$ may have multiple minima). It was found to be easier to optimize $A^2(t)$ than $A(t)$. Therefore, all of the results presented in the present works are obtained by optimizing $A^2(t)$.

### 2. Functional form control

For the optimal control of the susceptibility change as a function of time, we introduce an error functional which measures the deviation of the susceptibility change as a function of time from a desired shape. Let $f(t)$ represent the desired profile which is defined over some time interval $[T_i,T_j]$, then the error functional may be written as

$$I_e=\int_{T_i}^{T_j} w(t)[\Delta\kappa(t)-f(t)]^2\,dt, \tag{2.27}$$

where $w(t)$ is a weight function. The cost functional chosen, therefore, is

$$Q=L_e+\beta_f L_f+L_p, \tag{2.28}$$

where $L_p$ and $L_f$ are defined by Eqs. (2.22) and (2.24), respectively. The corresponding working formula for optimizing $A^2(t')$ is

$$\frac{\delta Q}{\delta A^2(t')}=\begin{cases}2\int_{T_i}^{T_j} w(t)[\Delta\kappa(t)-f(t)]\tilde{T}(t-t')dt+\dfrac{\delta(\beta_f L_f+L_p)}{\delta A^2(t')} & \text{for } 0<t'<T_j,\\ 0 \quad \text{otherwise,}\end{cases} \tag{2.29}$$

subject to Eq. (2.26b). In the numerical calculations to follow, the conjugate gradient algorithm was used for iteratively searching and constructing optimal fields. Detailed results will be presented in the next section for $CS_2$ gas.

## III. ILLUSTRATIONS

As an illustrative example, we consider the optimal control of the susceptibility change for $CS_2$ gas. The linear and symmetric molecule, $CS_2$, has a zero total nuclear spin. Therefore, only even $l$ rotational states can be populated. As a result, the odd summation in Eq. (2.21b) for $\tilde{T}(s)$ no longer exists. For $CS_2$, the rotational constant is small ($B=0.1091\ \text{cm}^{-1}$),[30] and the polarizability anisotropy is large with $\Delta\alpha=9.6\ \text{Å}^3$.[31]

In the following subsections, we present results of terminal optimal control and the functional optimal control of the susceptibility change for $CS_2$ gas in terms of a dimensionaless susceptibility change, $\Delta\kappa(t)$, defined by

$$\overline{\Delta\kappa}(t)\equiv\Delta\kappa(t)/(N_d\Delta\alpha)$$
$$=\text{Tr}[\cos^2(\theta)e^{-iH_0t}\rho_I^{(1)}(t)e^{iH_0t}]. \tag{3.1}$$

Here the temperature is assumed to be $T_m=300$ K. The effects of gas temperature or the initial Boltzmann distribution on the optimally controlled susceptibility changes will be discussed in Sec. III C. The amplitude, $A^2(t)$, is restrained with the bound value, $A_0^2=2.0\times10^{-10}$ a.u. ($\sim$7.0 MW/cm$^2$), while the energy fluence control is neglected by assigning $\beta_f=0$ in the cost functionals. For the terminal control case, we choose $\beta_0=0.1$ for the error function, $f_0=1.0$ for the desired value of $\overline{\Delta\kappa}(T)$ at a target time $t=T$, and $\beta_1=\beta_2=10^{10}$ for the amplitude control. For the functional form control of the susceptibility change, $\beta_1=\beta_2=1$ and the weight function $w(t)=10^4$ are utilized, unless specified otherwise.

### A. Optimal control of susceptibility change at time $T$

It is evident from Eqs. (2.21) that for a linear molecular gas $\tilde{T}(t)$ is a periodic function of time $t$ with a period $1/2B$, and characteristic time $1/8B$. For the terminal control cases, these times play an important role, which will become clear in the following results. For $CS_2$, $1/8B=38.2$ ps, and hence $1/2B=152.9$ ps.

Figures 1(a)–1(e) display the optimal fields with $f_0=1.0$ for target times $T=11.2$ ps, 49.4($=11.2+1/8B$) ps, 87.6($=11.2+1/4B$) ps, 125.8($=11.2+3/8B$) ps, and $T=152.9(=1/2B)$ ps, respectively. Three important features are evident in the figures. First, each of the optimal

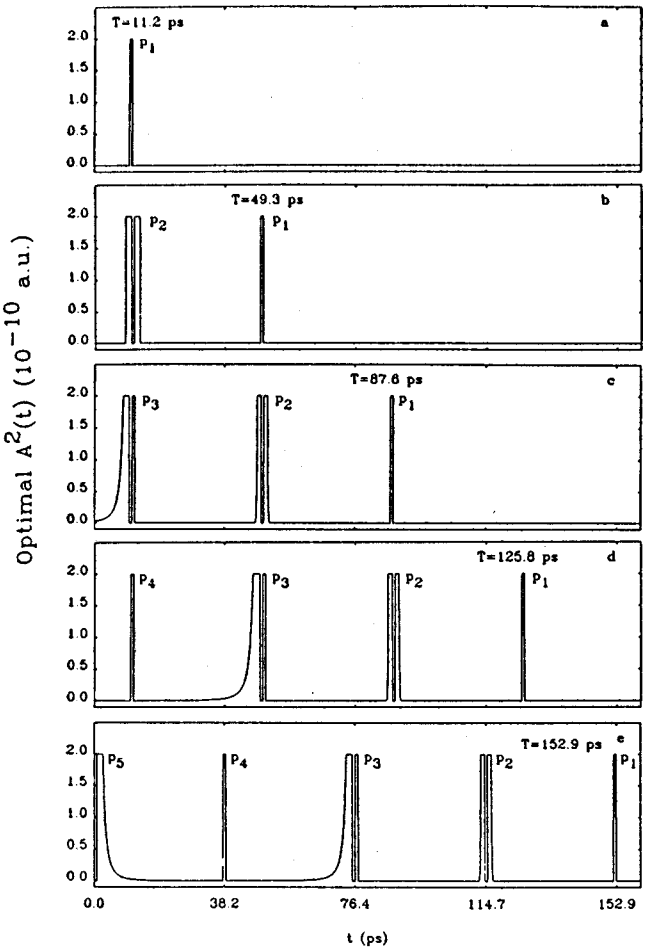


FIG. 1. The terminal control optimal fields for $CS_2$ gas at temperature $T_m=300$ K for the various target times (a) $T=11.2$ ps, (b) $T=49.4$ $(=11.2+1/8B)$ ps, (c) $T=87.6(=11.2+1/4B)$ ps, (d) $T=125.8$ $(=11.2+3/8B)$ ps, and (e) $T=152.9(=1/2B)$ ps, respectively, obtained under the bound restriction, $A^2(t)\leqslant 2\times 10^{-10}$ a.u. $B$ is the molecular rotational constant which is equal to 0.1091 $cm^{-1}$ for $CS_2$. These plots, together with the plot in Fig. 2, show that the optimal fields are a function of $(T-t)$ for the time interval $[0,T]$ with a characteristic time of $1/8B$ and a period of $1/2B$.

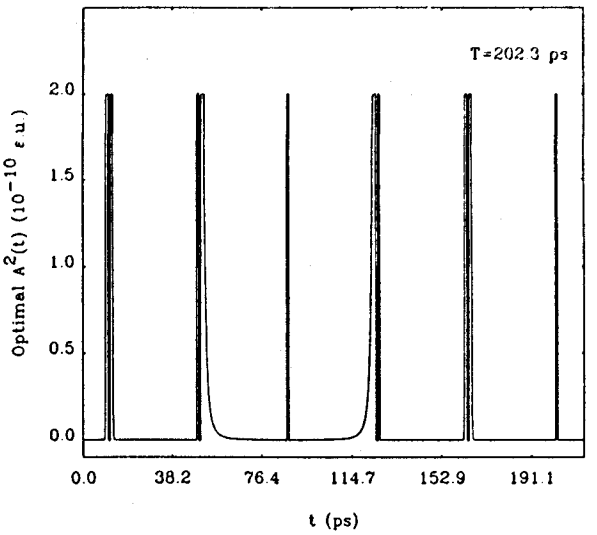


FIG. 2. The terminal control optimal field for $CS_2$ gas at temperature $T_m=300$ K for the target time $T=202.3(=11.2+5/8B)$ ps, longer than $1/2B$, obtained under the same bound restriction as the one for Figs. 1. The plot shows the periodic structures of the optimal field.

fields is composed of a set of rectangular (or quasirectangular) single and double pulses. Second, all of these optimized pulses satisfy the bound requirement, i.e., $A^2(t)\leqslant 2\times 10^{-10}$ a.u., and approach the bound value. Finally, the optimal fields are a function of $(T-t)$ for the time interval $[0,T]$. There is always a single pulse ending at the target time. The distance between any two neighboring pulses (single or double) is approximately $\sim 1/8B$. We can therefore classify these pulses into five types labeled by $p_1$, $p_2$, $p_3$, $p_4$, and $p_5$ in the figures. The following features of these types of pulses are observed: (1) the $p_1$ pulse is of width $\sim 0.8$ ps and always ends at a target time $T$ (here the pulse width is defined by the full width at half-maximum of the intensity); (2) The two pulses of the double pulse $p_2$ are of the same width $\sim 1.2$ ps, and one pulse is delayed by $\sim 0.8$ ps from the other. The center position of $p_2$ is $1/8B$ away from the target time $T$; (3) The second pulse in $p_3$ is of the same width as $p_1$. It is delayed by $\sim 0.8$ ps from the the first pulse and starts at the time $1/4B$ away from the target time $T$. The first pulse of $p_3$ has a relatively long rise time, and its typical width is $\sim 2.4$ ps; (4) The pulse $p_4$ has the same width as $p_1$ and the center position is $3/8B$ away from the target time $T$; (5) The pulse $p_5$ can be viewed as the image of the first pulse of $p_3$ reflected at the center of $p_4$ and starts at $\sim(T-0.8)$ ps.

Although the optimal fields shown in Figs. 1 are the ones for the indicated specific target times, they characterize the general behavior of optimal fields for other target times in those regions. In fact, for target times within the same region, e.g., $T<1/8B$, the optimal fields possess the same behavior. In other words, the shapes of optimal fields as a function of $(T-t)$ are the same, regardless of the particular target times in this region. We have also carried out extensive numerical studies for $T>1/2B$, and found that the optimal fields are always composed of the above mentioned five types of pulses and have a periodic structure with the period of $1/2B$. Figure 2 shows an example for $T=202.3(=11.2+5/8B)$ ps. An optimal field for $T>1/2B$ can be constructed in the following way. Letting $n$ be the number of complete periods that $T$ contains, the structure of the optimal field in $[T-n/2B,T]$ is the $n$th replica of the optimal field shown in Fig. 1(e), and in $[0,T-n/2B]$, it is the replica of the optimal field in the $[(n+1)/2B-T,1/2B]$ region.

Figure 3 presents the power spectrum of the optimal field shown in Fig. 1(c). One sees that the entire spectrum is in the microwave region. Physically, this is understandable, since the variations of $A^2(t)$ are dictated by molecular rotational transitions. It should be noted that the envelope of the spectral peaks mainly results from the narrowest pulse of the field, i.e., $p_1$, and modified by the other pulses in Fig. 1(c). The pulse $p_1$ has an approximate rectangular shape with width $\sim 0.8$ ps. The Fourier transform of $p_1$ is a zero-order Bessel function and the main peak has bandwidth $\sim 40$ $cm^{-1}$. The fine structure of the spectrum, with a width $\sim 0.87$ $cm^{-1}$, is determined by the distance of the

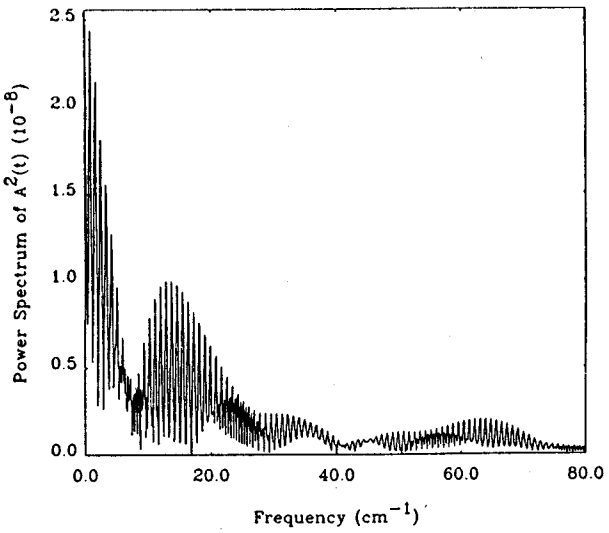


FIG. 3. The power spectrum of the optimal field $A^2(t)$ shown in Fig. 1(c). It characterizes the general features of the intensity-constrained optimal fields for the terminal control of the electric susceptibility change of $CS_2$ gas.

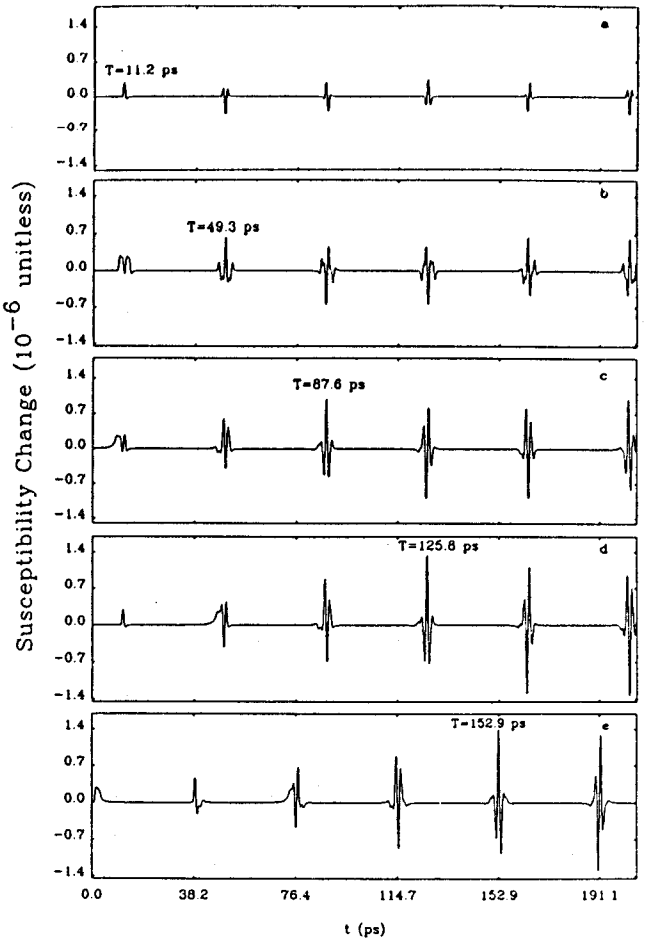


FIG. 4. The induced electric susceptibility changes of $CS_2$ gas under the optimal fields shown in Figs. 1(a)–1(e), respectively, at temperature $T_m = 300$ K.

neighboring pulses. Since all the optimal fields for the terminal controls have similar features, one can expect that their spectra should have similar features to the one shown in Fig. 3. Note that this power spectrum was calculated assuming that the phase $\vartheta(t)$ of the optical field is constant [see Eq. (2.1)]. The susceptibility change of the molecular gas depends only on the optical intensity profile and not on the phase profile; However, the power spectrum does depend on the assumed phase profile $\vartheta(t)$. Thus the power spectrum plotted in Fig. 3 is only one of many possible for a given $A^2(t)$. In some cases it may be useful to utilize a time-varying phase profile as a further degree of freedom, e.g., to obtain a smoother power spectrum. [This approach was in fact utilized in the work of Ref. 3, in which pulse shaping techniques[22] were used to convert individual femtosecond pulses into pulse sequences suitable for simple molecular control experiments. By choosing a proper set of phases $\vartheta(t)$, it was possible to achieve pulse sequences with the same power spectrum as the original femtosecond pulse, thus avoiding loss of energy in the pulse shaping process.]

The susceptibility changes induced by the optimal fields shown in Figs. 1 are presented in Figs. 4 as a function of time. It is seen that the susceptibility changes are steadily driven by the optimal fields from initially zero to a maximum at the given target time. After the target times the susceptibility changes evolve freely with a period of $1/2B$ and a characteristic time of $1/8B$. Comparing the susceptibility changes for various target times, one can observe that the longer the target time, the larger the susceptibility change can be. The achieved susceptibility changes, $\overline{\Delta\kappa}(T)$, are $\sim 2.9\times10^{-7}$ for $T=11.2$ ps, $\sim 6.4\times10^{-7}$ for $T=49.4$ ps, $\sim 9.9\times10^{-7}$ for $T=87.6$ ps, $\sim 13.4\times10^{-7}$ for $T=125.8$ ps, and $\sim 14.0\times10^{-7}$ for a complete period $T=152.9$ ps.

The above results can be understood by carefully examining Eq. (2.20a) and Eqs. (2.21). In Eq. (2.20a), it is shown that the susceptibility change of a molecular gas, $\Delta\kappa(T)$, is equal to the convolution of a driving field $A^2(t)$ and the function $\tilde{T}(t)$ over $[0,T]$. Naturally, the structure of $\tilde{T}(t)$ plays a key role in determining $\Delta\kappa(T)$. For a linear molecular gas the function $\tilde{T}(t)$, described by Eq. (2.21b), is proportional to the imaginary part of the Fourier transforms of $G_l$ multiplied by the phases, and is a temperature-dependent periodic function of $t$ with a period $1/2B$ and a characteristic time $1/8B$. For $CS_2$ gas, as mentioned before, all $G_l$ with odd angular momentum quantum numbers $l(=2j+1)$ equal zero because of symmetry. Figure 5 shows $\tilde{T}(t)$ as a function of time $t$ for $CS_2$ gas at the temperature 300 K, and one can see that it has both positive and negative peaks. Noting that $A^2(t)$ is a nonnegative function and considering the convolution relation, it is obvious that in order to maximize the terminal value of $\Delta\kappa(T)$, a control field, $A^2(T-t)$, must match the structure of $\tilde{T}(t)$ over the time interval $[0,T]$. Therefore, the optimal field $A^2(T-t)$ should have maximal overlap with all of the positively valued peaks of $\tilde{T}(t)$ and be zero at the negatively valued peaks of $\tilde{T}(t)$. Moreover, it has to satisfy the restraint upper bound condition. It is these factors that finally result in the special structures of the optimal fields.

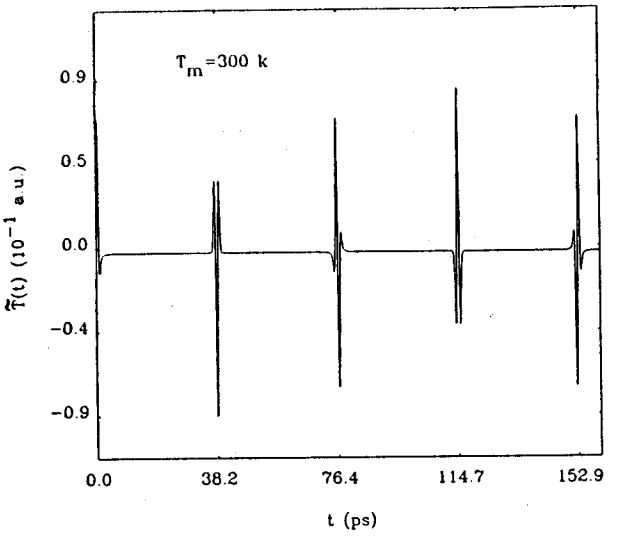


FIG. 5. The characteristic function $\tilde{T}(t)$ of the electric susceptibility change of a linear molecular gas under non-resonant optical fields, described by Eq. (2.21b), whose structures play a key role in determining the optimal control and the optimal fields properties. This plot is for $CS_2$.

Without any additional restriction on the control field, the best shape is rectangular for the pulses to assure the largest overlapes. The actual shapes of the optimized pulses shown in Figs. 1 and 2 deviate from the expected rectangles, due to the particular choice of the cost functional $Q$.

### B. Optimal control of temporal profiles of susceptibility change

We now proceed to discuss the optimal control of the temporal profiles of the susceptibility change in $CS_2$. As the first example, we consider the target profile

$$f(t)=\begin{cases}0 & \text{for} \quad 0\leqslant t<t_1\,,\\ f_0\sin^2[\pi(t-t_1)/a] & \text{for} \quad t_1\leqslant t<t_2\,,\\ f_0 & \text{for} \quad t_2\leqslant t<t_3\,,\\ f_0\sin^2[\pi(t-t_4)/a] & \text{for} \quad t_3\leqslant t<t_4\,,\\ 0 & \text{for} \quad t_4\leqslant t<t_5\,,\end{cases} \tag{3.2}$$

with $t_1=10.0$ ps, $t_2=11.0$ ps, $t_3=27.2$ ps, $t_4=28.2$ ps, $t_5=1/8B=38.2$ ps, $a=2.0$ ps and $f_0=10^{-8}$, which is displayed in Fig. 6(a) by the dashed line (virtually exactly overlapped by the achieved solid line optimal result). Physically, we wish to control the gas molecules by quickly (within $\sim$1 ps) orienting them in a desired fashion, then keep this orientation for 16.2 ps, and after $t_3$ quickly (within $\sim$1 ps) come back to the original isotropic state. The temporal profile of the susceptibility change induced by the optimal field is displayed in Fig. 6(a) by the solid line. It is seen that the target profile and the optimally reached profile coincide virtually exactly with each other! The temporal susceptibility change of the $CS_2$ gas sample can be controlled to almost exactly follow the target profile with the optimal field. The optimal field is given by the solid line in Fig. 6(b) and its power spectrum is shown in Fig. 7. Unlike the optimal field for a case of terminal control, which is composed of a set of rectangular pulses, the

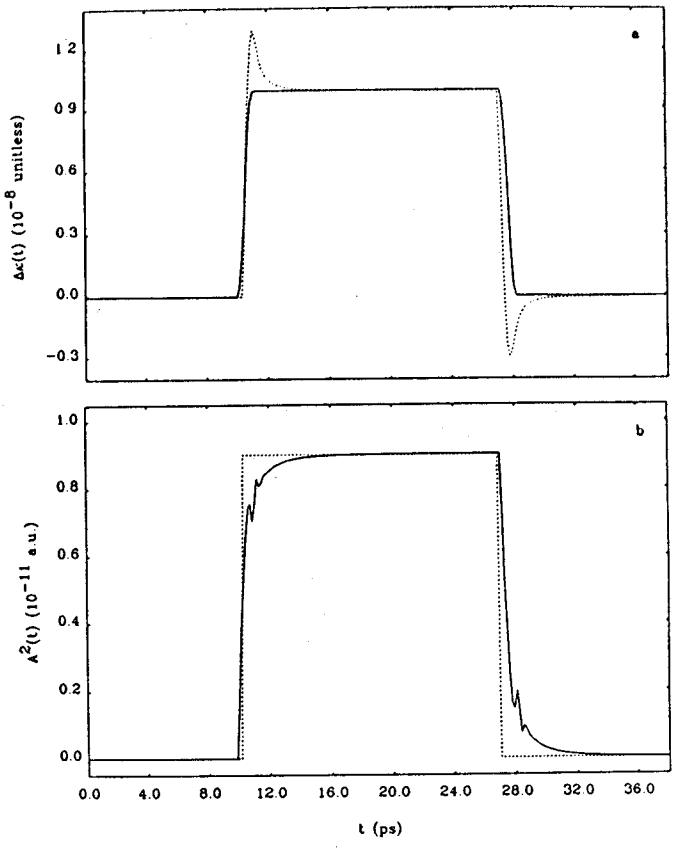


FIG. 6. The temporal profile control of the electric susceptibility change of $CS_2$ gas at $T_m=300$ K. The solid lines in (a) and (b) are, respectively, the optimally controlled susceptibility change profile and the corresponding optimal control field. The target profile is defined by Eq. (3.2) and plotted by the dashed line in (a) which is virtually exactly overlapped by the solid line to show that the desired target profile can be almost exactly approached. The dotted line in (a) is the result under the non-optimal field shown in *b* by the dotted line which explains the importance of the fine structure of the optimal field.

optimal field for profile control has a similar shape to the target profile. To understand the importance of the fine structure of optimal field, we have used the nonoptimal field presented in Fig. 6(b) by the dotted line as the driving

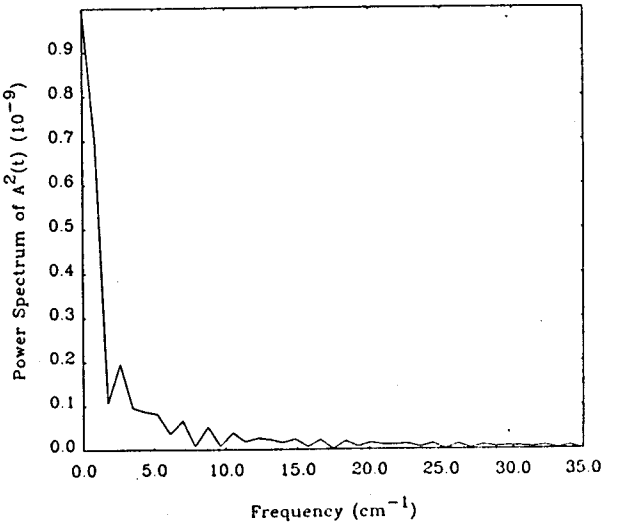


FIG. 7. The power spectrum of the optimal field $A^2(t)$ shown in Fig. 6(b).

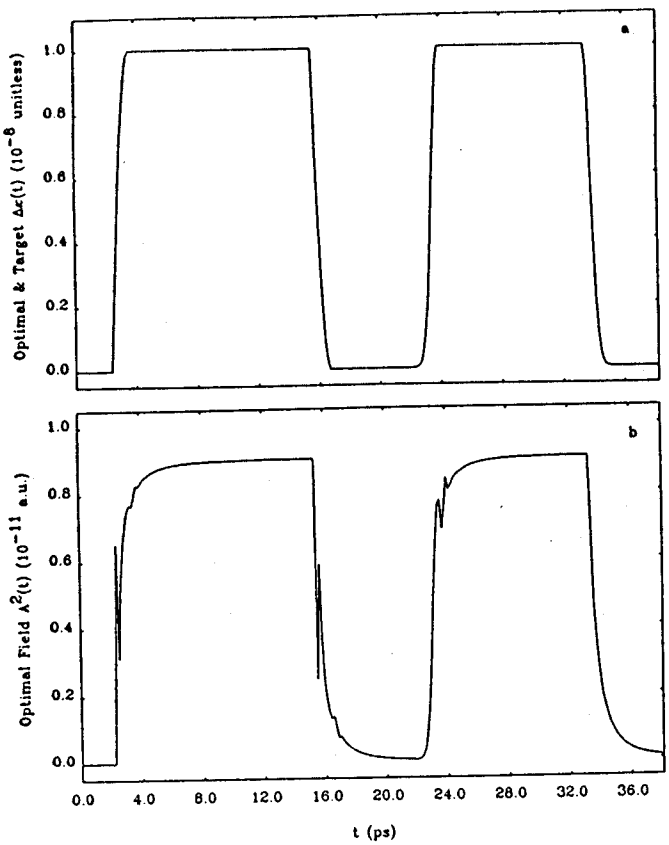


FIG. 8. The optimal control results of $CS_2$ gas at $T_m=300$ K for the target profile defined by Eq. (3.3) and plotted in (a) by the dashed line which is overlapped virtually exactly with the optimally achieved solid line. The corresponding optimal field is shown in (b).

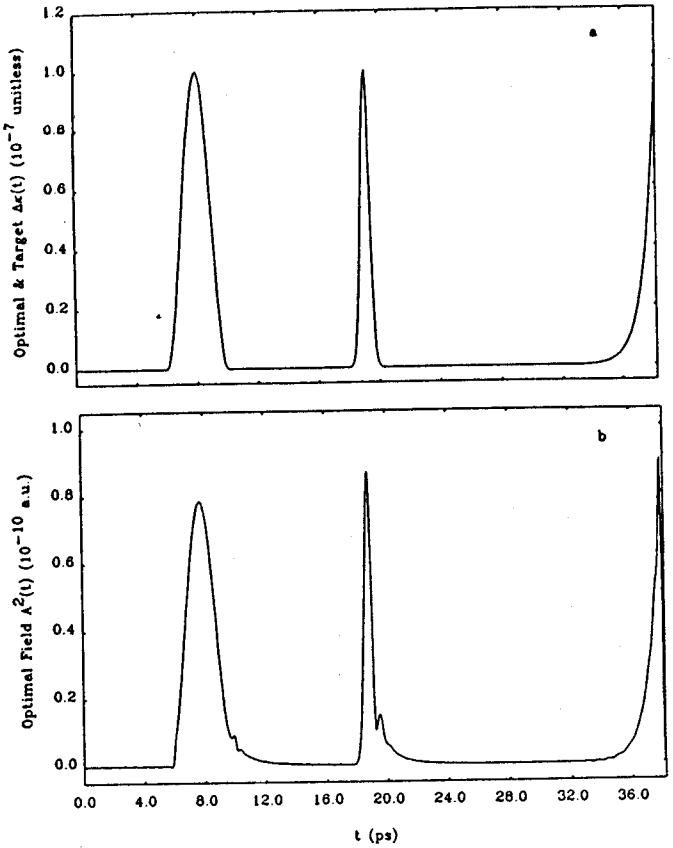


FIG. 9. The optimal control results of $CS_2$ gas at $T_m=300$ K for the target profile defined by Eq. (3.4) and plotted in (a) by the dashed line which is overlapped virtually exactly with the optimally achieved solid line. The corresponding optimal field is shown in (b).

field. The resultant temporal susceptibility change profile is shown in Fig. 6(a) by the dotted line. It is seen that the modified field without the detailed features does not give rise to the desired profile. Therefore, it is necessary to use the designed optimal field in order to achieve nearly perfect control. However, quite respectable results can be achieved by a square pulse in this case.

Next, we proceed to explore control for more complex profiles. First, we consider a target profile given below

$$f(t)=\begin{cases}0 & \text{for} \quad 0\leqslant t<t_1,\\ f_0\sin[\pi(t-t_1)/a] & \text{for} \quad t_1\leqslant t<t_2,\\ f_0 & \text{for} \quad t_2\leqslant t<t_3,\\ f_0\{1-\sin[\pi(t-t_3)/a]\} & \text{for} \quad t_3\leqslant t<t_4,\\ 0 & \text{for} \quad t_4\leqslant t<t_5,\\ f_0\exp[-(t-t_6)^2/b] & \text{for} \quad t_5\leqslant t<t_6,\\ f_0 & \text{for} \quad t_6\leqslant t<t_7,\\ f_0\exp[-(t-t_7)^2/b] & \text{for} \quad t_7\leqslant t<t_8,\\ 0 & \text{for} \quad t_8\leqslant t<t_9,\end{cases} \tag{3.3}$$

where $t_1=2.4$ ps, $t_2=3.6$ ps, $t_3=15.5$ ps, $t_4=16.7$ ps, $t_5=21.8$ ps, $t_6=23.9$ ps, $t_7=33.4$ ps, $t_8=35.5$ ps, $t_9=1/8B=38.2$ ps, $a=2.4$ ps, $b=2.4$ ps$^2$, and $f_0=10^{-8}$. Figure 8(a) depicts the target profile by the dashed line (overlapped virtually exactly with the optimally achieved solid line). The optimal control field is presented in in Fig. 8(b). Figure 8(a) shows that the desired temporal susceptibility change once again can be reached virtually exactly. We next consider a target profile consisting of three curves: a sinusoid, a Gaussian and an exponential:

$$f(t)=\begin{cases}0 & \text{for} \quad 0\leqslant t<t_1,\\ f_0\sin^2[\pi(t-t_1)/a] & \text{for} \quad t_1\leqslant t<t_2,\\ f_0\exp[-(t-t_3)^2/b] & \text{for} \quad t_2\leqslant t<t_4,\\ f_0\exp[-(t_5-t)/c] & \text{for} \quad t_4\leqslant t\leqslant t_5.\end{cases} \tag{3.4}$$

The target profile shown in Fig. 9(a) by the dashed line (and once again overlapping the optimal result) is calculated with parameters $t_1=6.0$ ps, $t_2=10.0$ ps, $t_3=19.1$ ps, $t_4=29.0$ ps, $t_5=38.2$ ps, $a=4.0$ ps, $b=0.4$ ps$^2$, $c=10.0$ ps, and $f_0=10^{-8}$. The optimal control field is displayed in Fig. 9(b). The nearly identical results of the target profile and the optimal profile shows that the desired profile can be well controlled.

The conclusions based on control of $CS_2$ above remain general, even though they are shown for special cases, under the condition that the target temporal profile is a smooth and non-negative function with "reasonable" maximal values and is localized within a time interval shorter than $1/8B$. This can be readily understood by carefully examining the convolution relation given in Eq. (2.20a),

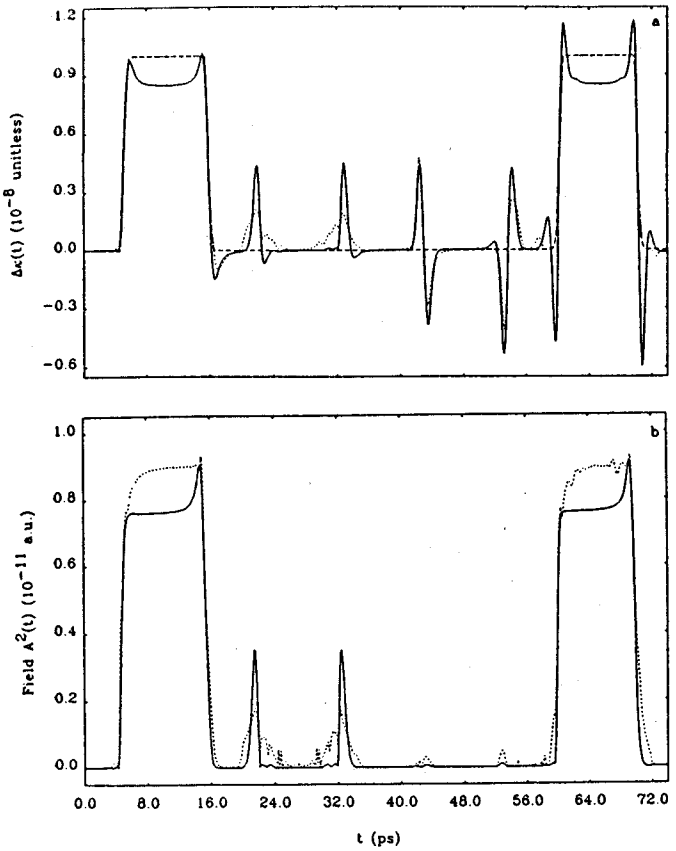


FIG. 10. The optimal control results of $CS_2$ gas at $T_m=300$ K for the target profile plotted in (a) by the dashed line. The solid lines in (a) and (b) are the optimal susceptibility change profile and optimal control field, respectively, under the weight function $w(t)=100$ defined over the time interval [0,74.0], while the dotted lines are the results under the weight function defined by Eq. (3.6).

the structure of $\tilde{T}(t)$ presented in Fig. 5, and the field amplitude restraint. We have carried out extensive numerical studies on the control of non-smooth profiles, e.g.,

$$f(t)=\begin{cases}0 & \text{for} \quad 0\leqslant t<t_1\,,\\ f_0 & \text{for} \quad t_1\leqslant t<t_2\,,\\ 0 & \text{for} \quad t_2\leqslant t<1/8B\,.\end{cases} \tag{3.5}$$

The calculated results show that they can not be controlled perfectly because the profiles are not smooth at some points. For instance, the purely rectangular profile, represented by Eq. (3.5), is discontinuous at $t_1$ and $t_2$. Physically, this behavior should not be surprising because any physical observable can not be changed at an infinite rate.

When a target profile is defined over a time interval longer than $1/8B$, it is usually difficult to achieve good control. To illustrate this, we choose the functions given by Eq. (3.3) as the target profile again, but with parameters $t_1=4.5$ ps, $t_2=5.5$ ps, $t_3=15.2$ ps, $t_4=16.2$ ps, $t_5=58.3$ ps, $t_6=60.5$ ps, $t_7=69.7$ ps, $t_8=71.8$ ps, $t_9=76.4$ ps, $a=2.4$ ps, $b=2.4$ ps$^2$, and $f_0=10^{-8}$. Figure 10(a) depicts the target profile by the dashed line. The optimal control field and temporal susceptibility change profile with $\beta_1=1$, $\beta_2=10^{10}$, and the weight function $w(t)=100$ defined over [0,74.0] ps are plotted in Fig. 10(b) and Fig. 10(a) by the solid lines, respectively. It is seen that the optimal field can not control the susceptibility change to accurately follow the target profile. The main reason is that in addition to the first set of peaks of $\tilde{T}(t)$ located near the initial time, the second set of peaks located at $\sim 1/8B$ are also affecting the susceptibility change. Thus the detailed assignment of the weight function $w(t)$ in the cost functional plays an important role in determining how to make the susceptibility change approach the target profile. For example, if we are particularly concerned with the profile in the regions II ($t_1\leqslant t<t_4$) and IV ($t_5\leqslant t<t_8$), shown in Fig. 10(a), the weight function can be chosen as

$$w(t)=\begin{cases}10^2 & \text{for} \quad 0\leqslant t<t_1\,,\\ 10^4 & \text{for} \quad t_1\leqslant t<t_4\,,\\ 10^2 & \text{for} \quad t_4\leqslant t<t_5\,,\\ 10^4 & \text{for} \quad t_5\leqslant t<t_8\,,\\ 10^2 & \text{for} \quad t_8\leqslant t<t_9\,,\end{cases} \tag{3.6}$$

with $t_i$ defined above. The calculated optimal field under $\beta_1=1$ and $\beta_2=10^8$ is presented in Fig. 10(b) and the resultant susceptibility change profile is displayed in Fig. 10(a) by the the dotted lines. Compared to the the solid line in Fig. 10(a), we see that the susceptibility change can now be much better controlled to follow the target profile in the regions II and IV (i.e., the achieved and desired results are indistinguishable in these regions).

Next, we examine a profile of a constant function defined over a time interval longer than $1/8B$. Physically, this is equivalent to requiring the achieved polarization to be retained for longer than $1/8B$. For convenience, we consider a target profile having the form of Eq. (3.2) with parameters $t_1=2.4$ ps, $t_2=3.6$ ps, $t_3=72.8$ ps, $t_4=74.0$ ps, $t_5=76.3$ ps, $a=2.4$ ps, and $f_0=10^{-8}$, as shown in Fig. 11(a) by the dashed line (closely overlapped by the solid line). The difference between this target profile and the one shown in Fig. 6 is that the latter has the constant function duration shorter than $1/8B$. The solid lines in Fig. 11(a) and Fig. 11(b) present the optimized susceptibility change profile and the optimal field, respectively, for $\beta_1=1$, $\beta_2=10^8$, and the weight function $w(t)=10^2$ over [0, 76.0] ps. It is evident that the desired constant profile can be well achieved. From Fig. 11(b), it is seen that except for the peaks in the middle, the optimal field overall behaves roughly like the susceptibility change profile. In order to understand the roles played by those peaks, as well as the importance of the detailed structure of the optimal field for the control, we employ a simplified nonoptimal field shown in Fig. 11(b) by the dotted line as a driving field. The dotted line in Fig. 11(a) depicts the resultant temporal susceptibility change. Obviously, the desired polarization is no longer retained; instead, there is an oscillation at about $1/8B$ away from the initial rise position $t_1$. The oscillation is caused by the second set of peaks (at $\sim 1/8B$) of $\tilde{T}(t)$. Therefore, we conclude that the role played by the peaks of the optimal field in Fig. 11(b) is to suppress the oscillations of the susceptibility change.

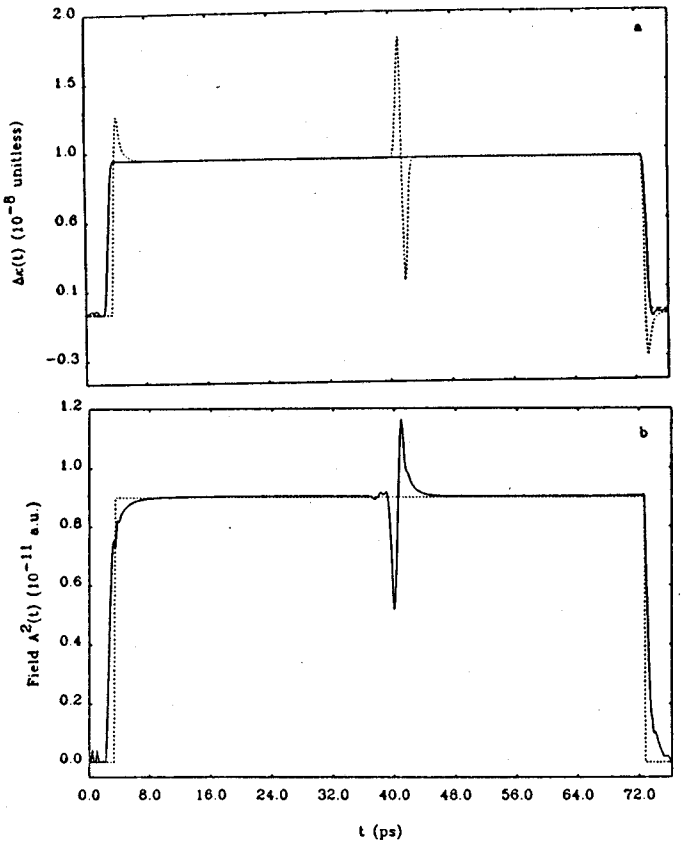


FIG. 11. The temporal profile control of the electric susceptibility change of $CS_2$ gas at $T_m=300$ K. The target profile is plotted by the dashed line in (a) (closely overlapped by the solid line). The solid lines in (a) and (b) are the optimal susceptibility change profile and the optimal control field, respectively. The dotted line in (a) is the result under the non-optimal field shown in (b) by the dotted line which shows the importance of the fine structure of the optimal field.

### C. Temperature effects on optimal control

The results shown are for the gas temperature of 300 K. Since the purpose of control is to change the system from an initial state to a desired state, the optimal control fields, as well as the optimal control results, accordingly, may be different as the gas temperature varies. A careful study of temperature effects shows that the characteristics of the optimal fields and the control of the susceptibility changes remain essentially the same. This is because temperature, in principle, only changes the population distribution among the molecular rotational states, or $G_l$. In other words, the gas temperature only affects the resolution of the oscillation peaks of $\tilde{T}(t)$, but not the entire relative structure. Generally, the higher the temperature is, the narrower the peaks of $\tilde{T}(t)$ are. As a consequence, for terminal control, the pulse widths of the optimal field become narrower, and thus the achieved terminal susceptibility change is smaller. For example, using the same cost functional as in Fig. 1(e) for the target time $T=152.9$ ps, the optimal terminal susceptibility change at 600 K is approximately half that at 300 K. For temporal profile control, increasing the temperature can smooth out the shapes of the optimal fields and wash out their oscillations.

## IV. CONCLUSIONS

In this paper, we presented results for optimal control of the electric susceptibility change of a homogeneous molecular gas with nonresonant lasers of low intensity. Two types of optimal control objectives have been taken into account: terminal control and temporal profile control. We carefully considered restrictions on the magnitude of the field amplitude, and introduced a step function into the cost functionals which helped to realize the amplitude restriction. $CS_2$ gas was utilized for the purpose of illustration. However, the general optimal control properties discussed for $CS_2$ can also be applied to other linear molecular gases with small rotational constants.

For terminal control of a maximal susceptibility change at a target time $T$, an optimal control field is usually composed of a series of rectangular pulses of the same amplitude equal to a preassigned bound value. The last pulse of the optimal field always ends at the target time, and any two neighboring pulses are separated from each other by $\sim 1/8B$ ps. Therefore, the number of pulses of an optimal field is completely determined by the length of $T$. The structure of the optimal fields is regular. If we let $T_1$ and $T_2$ be two different target times with $T_1$ shorter than $T_2$, then the entire structure of the optimal field for $T_1$ over $[0,T_1]$ coincides with the structure of the optimal field for $T_2$ over $[T_2-T_1,T_2]$. The time $1/2B$ serves as the period of an optimal field for $T>1/2B$, and is also the period of gas susceptibility free evolution. We have shown that for a desired target time $T$, the optimal field can drive the susceptibility change of $CS_2$ gas to achieve a maximal value exactly at $T$. In general, the longer the target time, the larger the maximally achievable value of the susceptibility change at the target time. However, if the difference between two target times is much smaller than $1/8B$, the maximally achievable values are identical. With a limited intensity laser ($\sim 7.0$ MW/cm$^2$) and a target time in the hundred picosecond range, the optimized susceptibility change of $CS_2$ gas is the order of $\overline{\Delta\kappa}(T) \sim 10^{-6}$.

For temporal profile control, the degree of control is very much dependent on the length of the time interval over which the target profile is defined. Usually if the time interval is shorter than $1/8B$ and the target profile is a smooth and non-negative function with a reasonable maximal value, the control usually can be realized perfectly. In other cases, the detailed assignment of the weight function in the cost functional plays an important role in determining how to make an optimally controlled susceptibility change profile approach a target profile.

It has been seen that the gas temperature can also affect the optimal control properties. For terminal control, the pulse widths of an optimal field and the maximally achievable susceptibility change are inversely proportional to the gas temperature, while for temporal profile control, a higher gas temperature will smooth out the functional form of the optimal field.

We have also shown the power spectra of the optimal fields, both for terminal controls and for temporal profile controls. For $CS_2$ gas at $T_m=300$ K, the power spectra

widths are less than a 100 $cm^{-1}$. Having a carrier frequency between $1 \sim 2 \times 10^4$ $cm^{-1}$, which is in the nonresonant region of $CS_2$, and frequency band width $\sim 10^2$ $cm^{-1}$, the required laser fields for optimal control of susceptibility changes for $CS_2$ gas appear feasible to achieve in the laboratory. It is the ultimate purpose of the present work to be preparatory for a molecular optimal control susceptibility change experiment.

## ACKNOWLEDGMENTS

One of the authors (H. R.) would like to acknowledge support from the Army Research Office, the Office of Naval Research, and the Air Force Office of Scientific Research.

[1] S. Conolly, D. Nishimura, and A. Maeovski, IEEE Med. Im. **5**, 106 (1986).
[2] M. McCoy and W. S. Warren, Chem. Phys. Lett. **133**, 165 (1987); W. S. Warren and M. S. Silver, Adv. Magn. Reson. **12**, 247 (1988); F. Loaiza, M. A. McCoy, S. L. Hammes, and W. S. Warren, J. Magn. Reson. **77**, 175 (1988).
[3] A. M. Weiner, D. E. Leaird, G. P. Wiederrecht, and K. A. Nelson, Science **247**, 1317 (1990); J. Opt. Soc. B **8**, 1264 (1991).
[4] C. P. Lin, J. Bates, J. T. Mayer, and W. S. Warren, J. Chem. Phys. **86**, 3750 (1987); F. C. Spano and W. S. Warren, Phys. Rev. A **37**, 1013 (1988); J. S. Melinger, A. Hariharan, S. R. Gandhi, and W. S. Warren, J. Chem. Phys. **95**, 2210 (1991).
[5] U. Gaubatz, P. Rudecki, M. Becker, S. Schiemann, M. Kulz, and K. Bergmann, Chem. Phys. Lett. **149**, 463 (1988).
[6] R. S. Judson, K. K. Lehmann, H. Rabitz, and W. S. Warren, Mol. Struct. **223**, 425 (1990); L. Shen and H. Rabitz, J. Phys. Chem. **95**, 1047 (1991).
[7] S. Shi, A. Woody, and H. Rabitz, J. Chem. Phys. **88**, 6870 (1988); A. P. Peirce, M. A. Dahleh, and H. Rabitz, Phys. Rev. A **37**, 4950 (1988); S. Shi and H. Rabitz, J. Chem. Phys. **92**, 364, 2927 (1990); Chem. Phys. **139**, 185 (1989); K. Yao, S. Shi, and H. Rabitz, *ibid.* **150**, 373 (1990); C. D. Schwieters, J. G. B. Beumee, and H. Rabitz, J. Opt. Soc. Am. B **7**, 1736 (1990); J. G. B. Beumee and H. Rabitz, J. Math. Phys. **31**, 1253 (1990); M. A. Dahleh, A. P. Peirce, and H. Rabitz, Phys. Rev. A **42**, 1065 (1990).
[8] G. K. Paramonov, Chem. Phys. Lett. **169**, 573 (1990).
[9] G. F. Thomas, J. Chem. Phys. **94**, 6928 (1991).
[10] S. Chelkowski, A. D. Bandrauk, and P. B. Corkum, Phys. Rev. Lett. **65**, 2355 (1990).
[11] J. J. Gerdy, M. Dantus, and R. M. Bowman, and A. H. Zewail, Chem. Phys. Lett. **171**, 1 (1990).
[12] N. F. Scherer, R. J. Carison, A. Matro, M. Du, A. J. Ruggiero, V. Romero-Rochin, J. A. Cina, G. R. Fleming, and S. A. Rice, J. Chem. Phys. **95**, 1487 (1991).
[13] P. Gross, D. Neuhauser, and H. Rabitz, J. Chem. Phys. **94**, 1158 (1991); C. D. Schwitcers and H. Rabitz, Phys. Rev. A **44**, 5224 (1991); S. Shi and H. Rabitz, Comput. Phys. Commun. **63**, 71 (1991).
[14] D. J. Tannor and S. A. Rice, J. Chem. Phys. **83**, 5013 (1985); D. J. Tannor, R. Kosloff, and S. A. Rice, *ibid.* **85**, 5805 (1986); S. A. Rice, D. J. Tannor, and R. Kosloff, J. Chem. Soc., Faraday Trans. 2 **82**, 2423 (1986); D. J. Tannor and S. A. Rice, Adv. Chem. Phys. **70**, 441 (1988).
[15] S. H. Tersigni, P. Gaspard, and S. A. Rice, J. Chem. Phys. **93**, 1670 (1990); B. Amstrup, R. J. Carlson, A. Matro, and S. A. Rice, *ibid.* **95**, 8019 (1991).
[16] M. Shapiro and P. Brumer, J. Chem. Phys. **84**, 4103 (1986); P. Brumer and M. Shapiro, Chem. Phys. Lett. **126**, 541 (1986); Faraday Discuss. Chem. Soc. **82**, 177 (1986); C. Asaro, P. Brumer, and M. Shapiro, Phys. Rev. Lett. **60**, 1634 (1988); M. Shapiro, J. W. Hepburn, and P. Brumer, Chem. Phys. Lett. **149**, 451 (1988); T. Seideman, M. Shapiro, and P. Brumer, J. Chem. Phys. **90**, 7132 (1989); M. Shapiro and P. Brumer, *ibid.* **90**, 6179 (1989); P. Brumer and M. Shapiro, Acc. Chem. Res. **22**, 407 (1989); Chem. Phys. **139**, 221 (1989); **144**, 146 (1990); J. L. Krause, M. Shapiro, and P. Brumer, J. Chem. Phys. **92**, 1126 (1990); I. Levy, M. Shapiro, and P. Brumer, *ibid.* **93**, 2493 (1990).
[17] S. Chelkowski and A. D. Bandrauk, Chem. Phys. Lett. **186**, 264 (1991).
[18] S. M. Park, S.-P. Lu, and R. J. Gordon, J. Chem. Phys. **94**, 8622 (1991).
[19] For example, R. B. Bernstein, *Chemical Dynamics via Molecular Beam and Laser Techniques* (Clarendon, New York, 1982).
[20] M. A. Duguay and J. W. Hansen, Appl. Phys. Lett. **15**, 192 (1969).
[21] A. M. Weiner, J. P. Heritage, and E. M. Kirschner, J. Opt. Soc. Am. B **5**, 1563 (1988); A. M. Weiner, J. P. Heritage, and J. A. Salehi, Opt. Lett. **13**, 300 (1988); A. M. Weiner, D. E. Leaird, J. S. Patel, and J. R. Wullert, *ibid.* **15**, 326 (1990); A. M. Weiner and D. E. Leaird, *ibid.* **15**, 51 (1990).
[22] M. Haner and W. S. Warren, Appl. Opt. **17**, 3687 (1987); Opt. Lett. **12**, 398 (1987); Appl. Phys. Lett. **52**, 1458 (1988); W. S. Warren, Science **242**, 878 (1988).
[23] J. A. Valdmanis, R. L. Fork, and J. P. Gordon, Opt. Lett. **10**, 131 (1985); C. P. Huang, H. C. Kapteyn, J. W. McIntosh, and M. M. Murnane, *ibid.* **17**, 139 (1992); M. Hofer, M. H. Ober, F. Haberl, and M. E. Fermann, IEEE J. Quantum Electron. **28**, 720 (1992).
[24] R. L. Fork, C. H. Brito Cruz, P. C. Becker, and C. V. Shank, Opt. Lett. **12**, 483 (1987).
[25] D. H. Reitze, A. M. Weiner, and D. E. Leaird, Appl. Phys. Lett. **61**, 1260 (1992).
[26] J. P. Heritage, T. K. Gustafson, and C. H. Lin, Phys. Rev. Lett. **34**, 1299 (1975).
[27] C. H. Lin, J. P. Heritage, and T. K. Gustafson, Appl. Phys. Lett. **19**, 397 (1971); C. H. Lin, J. P. Heritage, T. K. Gustafson, R. Y. Chiao, and J. P. Mctague, Phys. Rev. A **13**, 813 (1976).
[28] For example, H. W. Kroto, *Molecular Rotation Spectra* (Wiley, New York, 1975).
[29] For example, D. G. Luenberger, *Introduction to Dynamic System, Theory, Models, and Applications* (Wiley, New York, 1979).
[30] G. Hertzberg, *Infrared and Raman Spectra* (Van Nostrand-Reinhold, New York, 1966).
[31] C. H. Rhee, R. M. Metzger, and F. M. Wiygul, J. Chem. Phys. **77**, 899 (1982).